

Likelihood techniques for the combined analysis of CMB temperature and polarisation power spectra.

W.J. Percival¹ & M.L. Brown²

¹ Institute of Cosmology and Gravitation, University of Portsmouth, Portsmouth, PO1 2EG

² Institute for Astronomy, University of Edinburgh, Blackford Hill, Edinburgh EH9 3HJ

25 May 2019

ABSTRACT

We consider the shape of the likelihood and posterior surfaces to be used when fitting cosmological models to CMB temperature and polarisation power spectra measured from experiments. In the limit of an all-sky survey with Gaussian distributed pixel noise we show that the true combined likelihood of the four CMB power spectra (TT, TE, EE & BB) has a Wishart distribution and we discuss the properties of this function. We compare various fits to the posterior surface of the C_{ls} , both in the case of a single auto-power spectrum and for a combination of temperature and polarisation data. In the latter case, it is important that the fits reduce to the Wishart distribution in the limit of near full-sky coverage. Simple extensions of auto-power spectrum fits to include polarisation data generally fail to match correlations between the different power spectra in this limit. Directly fitting pixel values on large scales, as undertaken by the WMAP team in their analysis of the 3 year data, avoids the complications of characterising the shape of the posterior for the power spectra. Finally we demonstrate the importance of the posterior distribution shape on analytic marginalisation, and provide a formula for analytic marginalisation over a calibration error given an all-sky survey.

Key words: methods: statistical - methods: analytical - cosmology: theory - cosmic microwave background

1 INTRODUCTION

In this era of precision cosmology (Spergel et al. 2003, 2006), it is vital that care is taken with every step involved in the analysis and interpretation of cosmological data. In this paper we consider the likelihood technique used to fit cosmological models to CMB power spectra. For their analysis of the 3-year data (Hinshaw et al. 2006; Page et al. 2006), the WMAP team have adopted a pixel-based likelihood analysis at low multipoles, thus avoiding the complications introduced by fitting to the shape of the posterior surface (Slosar et al. 2004). This posterior surface is strongly non-Gaussian which must be accounted for when performing model comparisons using power spectra. In addition, there are now important constraints on both the temperature and polarisation power spectra, which are not independent and need to be jointly analysed.

In this paper we review previous work analysing the posterior surface for temperature power spectra and extend this to include polarisation data. Initially, we present exact formulae for all-sky surveys with negligible noise. The inclusion of uncorrelated Gaussian distributed pixel noise will not change the form of the posterior surface for the C_{ls} as it will simply increase the variance in the a_{lms} – to calculate the C_{ls} we are still summing the squares of Gaussian random variables. However, an incomplete sky map will change the posterior distribution, causing correlations between modes, and will also change the posterior shape. For any survey, the central limit theorem can be invoked to show that at large l , the likelihood distribution will tend to a multi-variate Gaussian form. We therefore see that the true likelihood will interpolate between a skewed distribution on large scales, and a multi-variate Gaussian distribution on small scales. Fitting formulae which are able to match this intrinsic change in shape have previously been adopted to provide an approximate likelihood calculation for a single auto-power spectrum. The primary aim of our paper is to extend these fits to the combination of temperature and polarisation data.

The layout of our paper is as follows. In Section 2 we lay the groundwork by briefly reviewing the standard Bayesian approach to model

* E-mail: will.percival@port.ac.uk, mlb@roe.ac.uk

selection, using Bayes theorem to link the likelihood to the posterior of interest. In Section 3.1 we review the well known likelihood and posterior distributions for the TT power spectrum of an all-sky noiseless survey. This work is expanded in Section 3.2 to include polarisation data in the same limit of no noise and an all-sky survey – the combined likelihood is given by the Wishart distribution. The important properties, including the multi-variate Gaussian limit at large l are presented. In Section 4 we discuss the complications introduced by realistic surveys on the posterior shape. These complications have led previous studies to consider posterior fits for the TT power spectrum, the most common of which is the log-normal distribution (Bond, Jaffe & Knox 2000). A number of these fits to the posterior surface are compared in Section 5.1. The extension of these fits to the joint analysis of temperature and polarisation data is considered in Section 5.2. The importance of this work setting the mathematical foundation for the shape of the posterior surface is demonstrated in Section 6, where we consider marginalising over a Gaussian distributed calibration error in the TT power spectrum. The difference between assuming a Gaussian posterior, commonly used in the literature, and using the correct distribution for an all-sky survey is demonstrated. We discuss our results in Section 7.

2 LIKELIHOODS AND POSTERIORS

Although it is probably the most reprinted equation in scientific literature, it is central to the work presented here, so for completeness we include the standard Bayesian equation

$$f(\mathbf{X}|\hat{\mathbf{X}}) = \frac{f(\hat{\mathbf{X}}|\mathbf{X})f(\mathbf{X})}{f(\hat{\mathbf{X}})}, \quad (1)$$

which relates the likelihood function $f(\hat{\mathbf{X}}|\mathbf{X})$ – the distribution of the data $\hat{\mathbf{X}}$ given a model \mathbf{X} , to the posterior $f(\mathbf{X}|\hat{\mathbf{X}})$ – the distribution of models given the data. The prior $f(\mathbf{X})$, which cannot be avoided, provides the information that we already know about the models. For example, our prior might be that only 6-parameters are needed to model present CMB data, and that we initially know nothing about those parameters – they themselves have uniform priors. Note that a uniform prior in the cosmological parameters does not translate to a uniform prior in the power spectra values. It is probably also worth emphasising that the distributions of the likelihood and posterior can have different forms. For example, if the likelihood is Gaussian, but has a variance that depends on the model, then the posterior will not be Gaussian, for a uniform prior on the models. We must therefore take care to distinguish likelihood and posterior.

In this work, we will quantify the data $\hat{\mathbf{X}}$ using the power spectra measured from some experiment, and the models \mathbf{X} by the same statistic. For an all-sky survey, where different modes are independent, the likelihood is

$$f(\hat{\mathbf{X}}|\mathbf{X}) = \prod_l f(\hat{C}_l^{\text{XX}}|C_l^{\text{XX}}), \quad (2)$$

where \hat{C}_l^{XX} represents the measured power spectra, C_l^{XX} the model power spectra, and XX = TT, EE, TE, BB. The posterior that we are interested in, $f(\mathbf{X}|\hat{\mathbf{X}})$ is dependent on the product of the likelihoods of individual multipoles. For a single multipole, we see that it is the dependence of the likelihood on the model power spectrum (C_l^{XX}) that is of interest. In this paper we refer to $f(C_l^{\text{XX}}|\hat{C}_l^{\text{XX}})$ as the posterior for the power spectra, as it is related to $f(\hat{C}_l^{\text{XX}}|C_l^{\text{XX}})$ using Bayes theorem and a uniform prior on $f(C_l^{\text{XX}})$. For a given experiment, it is the posterior $f(C_l^{\text{XX}}|\hat{C}_l^{\text{XX}})$ that tells us the model constraints provided by the data on a particular scale.

3 LIKELIHOOD AND POSTERIOR DISTRIBUTIONS FOR ALL-SKY NOISELESS SURVEYS

3.1 Temperature only data

In an all-sky, noiseless CMB survey, the Spherical Harmonic coefficients a_{lm}^{T} of the temperature fluctuations obey a Gaussian distribution

$$f(a_{lm}^{\text{T}}|C_l^{\text{TT}}) = \frac{1}{\sqrt{2\pi C_l^{\text{TT}}}} \exp\left[-\frac{|a_{lm}^{\text{T}}|^2}{2C_l^{\text{TT}}}\right], \quad (3)$$

where $C_l^{\text{TT}} = \langle |a_{lm}^{\text{T}}|^2 \rangle$. Using statistical isotropy, we can average over m and define an estimator of the power

$$\hat{C}_l^{\text{TT}} = \frac{1}{2l+1} \sum_m |a_{lm}^{\text{T}}|^2. \quad (4)$$

The sum of the squares of ν standard Gaussian random variables has a χ^2 distribution with ν degrees of freedom. Consequently, $\hat{Y}_l = \sum_m |a_{lm}^{\text{T}}|/\sqrt{C_l^{\text{TT}}}$ will have a χ^2 distribution with $\nu = 2l+1$ degrees of freedom

$$f(\hat{Y}_l|C_l^{\text{TT}}) = \frac{\hat{Y}_l^{\nu/2-1}}{\Gamma(\nu/2)2^{\nu/2}} \exp\left[-\frac{\hat{Y}_l}{2}\right]. \quad (5)$$

\hat{C}_l^{TT} is a multiple of \hat{Y}_l , $\hat{C}_l^{\text{TT}} = C_l^{\text{TT}}\hat{Y}_l/\nu$ so the likelihood will have a Γ distribution

$$f(\hat{C}_l^{\text{TT}}|C_l^{\text{TT}}) \propto C_l^{\text{TT}} \left(\frac{\hat{C}_l^{\text{TT}}}{C_l^{\text{TT}}}\right)^{\nu/2-1} \exp\left[-\frac{\nu\hat{C}_l^{\text{TT}}}{2C_l^{\text{TT}}}\right]. \quad (6)$$

The mean and variance of this distribution are C_l^{TT} and $2(C_l^{\text{TT}})^2/\nu$. Note that the maximum of this distribution occurs at $(\nu - 2)/\nu C_l^{\text{TT}}$, not at the mean value. In the limit $\nu \rightarrow \infty$, the central limit theorem gives that this distribution tends towards a Gaussian with the same mean and variance.

Using Bayes theorem to convert to the posterior $f(C_l^{\text{TT}}|\hat{C}_l^{\text{TT}})$, assuming a uniform prior in $f(C_l^{\text{TT}})$ gives

$$f(C_l^{\text{TT}}|\hat{C}_l^{\text{TT}}) \propto (C_l^{\text{TT}})^{-\nu/2} \exp\left[-\frac{\nu \hat{C}_l^{\text{TT}}}{2C_l^{\text{TT}}}\right], \quad (7)$$

where we have not included the normalisation factor dependent on \hat{C}_l^{TT} . The maximum of this function occurs at \hat{C}_l^{TT} , while the mean is given by

$$\langle C_l^{\text{TT}} \rangle = \frac{\nu}{\nu - 4} \hat{C}_l^{\text{TT}}. \quad (8)$$

This offset between maximum and mean is simply a result of the skewness of the distribution. As $\nu \rightarrow \infty$, this distribution will tend towards a Gaussian form. This follows from the Bayesian identity and the fact that $f(\hat{C}_l^{\text{TT}}|C_l^{\text{TT}})$ tends to a Gaussian distribution (see the discussion following equation (28)).

We can take the logarithm of the posterior to give

$$-\ln f(C_l^{\text{TT}}|\hat{C}_l^{\text{TT}}) = \frac{\nu}{2} (\ln C_l^{\text{TT}} + \hat{C}_l^{\text{TT}}/C_l^{\text{TT}}), \quad (9)$$

ignoring an irrelevant additive constant. From this, we can calculate the curvature around the distribution maximum

$$-\frac{d^2 \ln f(C_l^{\text{TT}}|\hat{C}_l^{\text{TT}})}{d^2 C_l^{\text{TT}}} \Big|_{\hat{C}_l^{\text{TT}}} \propto \frac{1}{(\hat{C}_l^{\text{TT}})^2}. \quad (10)$$

There is an alternative way of deriving equation (9) by considering the joint probability density of a_{lm}^{T} for $-l \leq m \leq l$,

$$f(a_{l,m=-l}^{\text{T}}, \dots, a_{l,m=l}^{\text{T}}|C_l^{\text{TT}}) = \prod_m f(a_{lm}^{\text{T}}|C_l^{\text{TT}}). \quad (11)$$

Substituting for $f(a_{lm}^{\text{T}}|C_l^{\text{TT}})$ from equation (3), this reduces to

$$-\ln f(C_l^{\text{TT}}|\hat{C}_l^{\text{TT}}) = \frac{1}{2} \sum_m (\ln C_l^{\text{TT}} + |a_{lm}^{\text{T}}|^2/C_l^{\text{TT}}), \quad (12)$$

where once again, we have ignored an irrelevant additive component. We see that this distribution is only dependent on a_{lm}^{T} through \hat{C}_l^{TT} , and that substituting in \hat{C}_l^{TT} from equation (4) leads to the same C_l^{TT} dependence that we had in equation (9).

3.2 Including polarisation data

If we now include E-mode and B-mode polarisation data, there are 3 spherical harmonic coefficients of interest, a_{lm}^{T} , a_{lm}^{E} and a_{lm}^{B} . These are multivariate Gaussian random variables with expected values of zero. The data vector \mathbf{X}_a and covariance matrix \mathbf{V}_l for the multivariate Gaussian can be written as

$$\mathbf{X}_a = \begin{pmatrix} a_{lm}^{\text{T}} \\ a_{lm}^{\text{E}} \\ a_{lm}^{\text{B}} \end{pmatrix}, \quad \mathbf{V}_l = \begin{pmatrix} C_l^{\text{TT}} & C_l^{\text{TE}} & 0 \\ C_l^{\text{TE}} & C_l^{\text{EE}} & 0 \\ 0 & 0 & C_l^{\text{BB}} \end{pmatrix}. \quad (13)$$

Note that the cross-correlations between different parity fields are expected to be zero (and B has the opposite parity to E and T). The random variables of interest are the elements of the matrix

$$\mathbf{S}_l = \frac{1}{2l+1} \sum_m \mathbf{X}_a \mathbf{X}_a^\dagger = \begin{pmatrix} \hat{C}_l^{\text{TT}} & \hat{C}_l^{\text{TE}} & \hat{C}_l^{\text{TB}} \\ \hat{C}_l^{\text{TE}} & \hat{C}_l^{\text{EE}} & \hat{C}_l^{\text{EB}} \\ \hat{C}_l^{\text{TB}} & \hat{C}_l^{\text{EB}} & \hat{C}_l^{\text{BB}} \end{pmatrix}, \quad (14)$$

where \mathbf{X}_a^\dagger represents the Hermitian conjugate of \mathbf{X}_a . The matrix \mathbf{S}_l has a Wishart distribution with $\nu = (2l+1)$ degrees of freedom. There is a slight complication caused by defining \mathbf{S}_l as the average over the $(2l+1)$ modes rather than the sum, which is used to derive the standard Wishart distribution. \mathbf{S}_l still has a Wishart distribution, but we need to consider the matrix $\mathbf{W}_l = \mathbf{V}_l/(2l+1)$ rather than \mathbf{V}_l . The Wishart distribution is given by

$$f(\mathbf{S}_l|\mathbf{W}_l) = \frac{|\mathbf{S}_l|^{(\nu-p-1)/2} \exp[-\text{trace}(\mathbf{W}_l^{-1} \mathbf{S}_l/2)]}{2^{p\nu/2} |\mathbf{W}_l|^{\nu/2} \Gamma_p(\nu/2)}, \quad (15)$$

where \mathbf{S}_l and \mathbf{W}_l are positive definite symmetric $p \times p$ matrices, $\nu > p$, and $\Gamma_p(\nu/2)$ is the multi-variate Gamma function,

$$\Gamma_p(\nu/2) = \pi^{p(p-1)/4} \prod_{i=1}^p \Gamma[(\nu + 1 - i)/2]. \quad (16)$$

Because of the form of \mathbf{V}_l , we can decompose into two Wishart distributions, one with $p = 2$ for \hat{C}_l^{TT} , \hat{C}_l^{EE} , \hat{C}_l^{TE} and a separate, independent, $p = 1$ Wishart distribution for \hat{C}_l^{BB} , which reduces to a Γ distribution as described in the previous Section. To help to understand the form of the Wishart distribution, we now explain how it is normalised, focusing on the $p = 2$ distribution covering \hat{C}_l^{TT} , \hat{C}_l^{EE} and \hat{C}_l^{TE} . The probability density function for \mathbf{S}_l is equivalent to the joint distribution of the elements of the matrix, over all positive definite matrices so

$$\int_0^\infty d\hat{C}_l^{\text{TT}} \int_0^\infty d\hat{C}_l^{\text{EE}} \int_{-\sqrt{\hat{C}_l^{\text{TT}}\hat{C}_l^{\text{EE}}}}^{+\sqrt{\hat{C}_l^{\text{TT}}\hat{C}_l^{\text{EE}}}} d\hat{C}_l^{\text{TE}} f(\mathbf{S}_l | \mathbf{V}_l) = 1. \quad (17)$$

As expected, the marginal distributions of the diagonal elements of \mathbf{S}_l have a Γ distribution as described in Section 3.1. However, the same is not true for the off-diagonal elements. First, suppose that we have obtained \hat{C}_l^{TT} and \hat{C}_l^{TE} , but for some reason not \hat{C}_l^{EE} (as for example with the WMAP year 1 data Bennett et al. 2003; Hinshaw et al. 2003). The joint likelihood of \hat{C}_l^{TT} and \hat{C}_l^{TE} can be obtained by integrating equation (15), with $p = 2$, over \hat{C}_l^{EE} forcing \mathbf{S}_l to be positive definite. The marginal distribution of \hat{C}_l^{TT} with the constraint $0 < \hat{C}_l^{\text{TT}} < \infty$, and \hat{C}_l^{TE} with the constraint $-\infty < \hat{C}_l^{\text{TE}} < \infty$ is

$$f(\hat{C}_l^{\text{TT}}, \hat{C}_l^{\text{TE}} | C_l^{\text{TT}}, C_l^{\text{TE}}, C_l^{\text{EE}}) = \frac{\nu^{(\nu+1)/2}}{\sqrt{\pi} \Gamma(\nu/2) 2^{\frac{\nu-1}{2}} |V|^{1/2}} \frac{(\hat{C}_l^{\text{TT}})^{(\nu-3)/2}}{(C_l^{\text{TT}})^{(\nu-1)/2}} \exp \left[-\frac{\nu}{2|V|} \left(\hat{C}_l^{\text{TT}} C_l^{\text{EE}} - 2\hat{C}_l^{\text{TE}} C_l^{\text{TE}} + \frac{(\hat{C}_l^{\text{TE}})^2 C_l^{\text{TT}}}{\hat{C}_l^{\text{TT}}} \right) \right]. \quad (18)$$

It is interesting to note that a constraint on \hat{C}_l^{TT} and \hat{C}_l^{TE} still leaves us with a likelihood that is dependent on C_l^{EE} – information is retained in this case. In fact, were we presented with an all-sky survey with negligible noise, then the likelihood analysis of any two or more of the three possible E and T mode auto- and cross-power spectra should be attempted using the full matrix \mathbf{V} .

By integrating equation (18) over \hat{C}_l^{TT} , we obtain the following marginal distribution for \hat{C}_l^{TE}

$$f(\hat{C}_l^{\text{TE}} | C_l^{\text{TT}}, C_l^{\text{TE}}, C_l^{\text{EE}}) = \frac{\nu}{\sqrt{\pi} \Gamma(\nu/2) 2^{\frac{\nu-1}{2}} |V|^{1/2}} \left[\frac{(\nu \hat{C}_l^{\text{TE}})^2}{C_l^{\text{TT}} C_l^{\text{EE}}} \right]^{(\nu-1)/4} \exp \left(\frac{\nu \hat{C}_l^{\text{TE}} C_l^{\text{TE}}}{|V|} \right) K_{(\nu-1)/2} \left(\frac{\nu |\hat{C}_l^{\text{TE}}| \sqrt{C_l^{\text{TT}} C_l^{\text{EE}}}}{|V|} \right), \quad (19)$$

where K_n is a modified Bessel function of the second kind, and $|V| = C_l^{\text{TT}} C_l^{\text{EE}} - (C_l^{\text{TE}})^2$. This marginal distribution covers the interval $-\infty < \hat{C}_l^{\text{TE}} < \infty$. Again it is worth emphasising that the likelihood is dependent on C_l^{TT} and C_l^{EE} in addition to C_l^{TE} . In a Bayesian analysis, the model constraint provided by a measurement of \hat{C}_l^{TE} depends on all of these model values.

The marginal distributions of \hat{C}_7^{TT} , \hat{C}_7^{EE} , \hat{C}_7^{TE} and \hat{C}_7^{BB} are plotted in Fig. 1 for the best-fit cosmological model of the WMAP year-1 data (Spergel et al. 2003) where we have included a B-mode polarisation component with an input tensor-to-scalar ratio of $T/S = 0.05$. These distributions were calculated from all-sky realisations of cosmological power spectra calculated using the CMBFAST (Seljak & Zaldarriaga 1996) and HEALPIX (Górski et al. 2005) packages. For comparison we plot the distributions predicted by equation (6) for the auto power spectra and equation (19) for the TE cross power spectrum, which show excellent agreement with the simulated data.

For the Wishart distribution, if we define the data vectors of interest by

$$\hat{\mathbf{X}}_C = \begin{pmatrix} \hat{C}_l^{\text{TT}} \\ \hat{C}_l^{\text{TE}} \\ \hat{C}_l^{\text{EE}} \end{pmatrix}, \quad \mathbf{X}_C = \begin{pmatrix} C_l^{\text{TT}} \\ C_l^{\text{TE}} \\ C_l^{\text{EE}} \end{pmatrix}, \quad (20)$$

then the covariance matrix for $\hat{\mathbf{X}}_C$ is given by

$$\mathbf{Y} = \frac{1}{\nu} \begin{pmatrix} 2(C_l^{\text{TT}})^2 & 2C_l^{\text{TT}} C_l^{\text{TE}} & 2(C_l^{\text{TE}})^2 \\ 2C_l^{\text{TT}} C_l^{\text{TE}} & C_l^{\text{TT}} C_l^{\text{EE}} + (C_l^{\text{TE}})^2 & 2C_l^{\text{TE}} C_l^{\text{EE}} \\ 2(C_l^{\text{TE}})^2 & 2C_l^{\text{TE}} C_l^{\text{EE}} & 2(C_l^{\text{EE}})^2 \end{pmatrix}. \quad (21)$$

As expected, the variance for the auto-power spectra matches that of the Γ distribution discussed in equation (6). However, the variance of the distribution in \hat{C}_l^{TE} has a different form, reflecting the change in marginalised distribution (equation (19) rather than a Γ distribution).

In the limit $\nu \rightarrow \infty$, the Wishart distribution tends towards a multi-variate Gaussian form, with the same covariance matrix. It is worth noting that the matrix \mathbf{Y} is also the curvature matrix around the distribution maximum, which will become important in Sections 5.1 and 5.2.

4 COMPLICATIONS FOR MORE REALISTIC SURVEYS

As discussed in the previous Section, the posterior distribution for a noise-less all-sky survey does not have a multi-variate Gaussian form in the auto- and cross- power spectra at low ν . The situation is more complicated for realistic data that includes effects such as noise, beam uncertainties, calibration errors and limited sky coverage. Such effects are often dealt with by modifying the posterior distribution to match that found from detailed simulations of the particular experiment being considered (e.g. Hivon et al. 2002). This modified distribution can, in turn, be fitted by simple functional forms, thus allowing rapid calculation for any given cosmological model (e.g. Bond, Jaffe & Knox 2000). In this Section we briefly examine the effect of real-world complications on the posterior, which provide the motivation for our consideration of possible fits for the posterior distribution in Section 5.

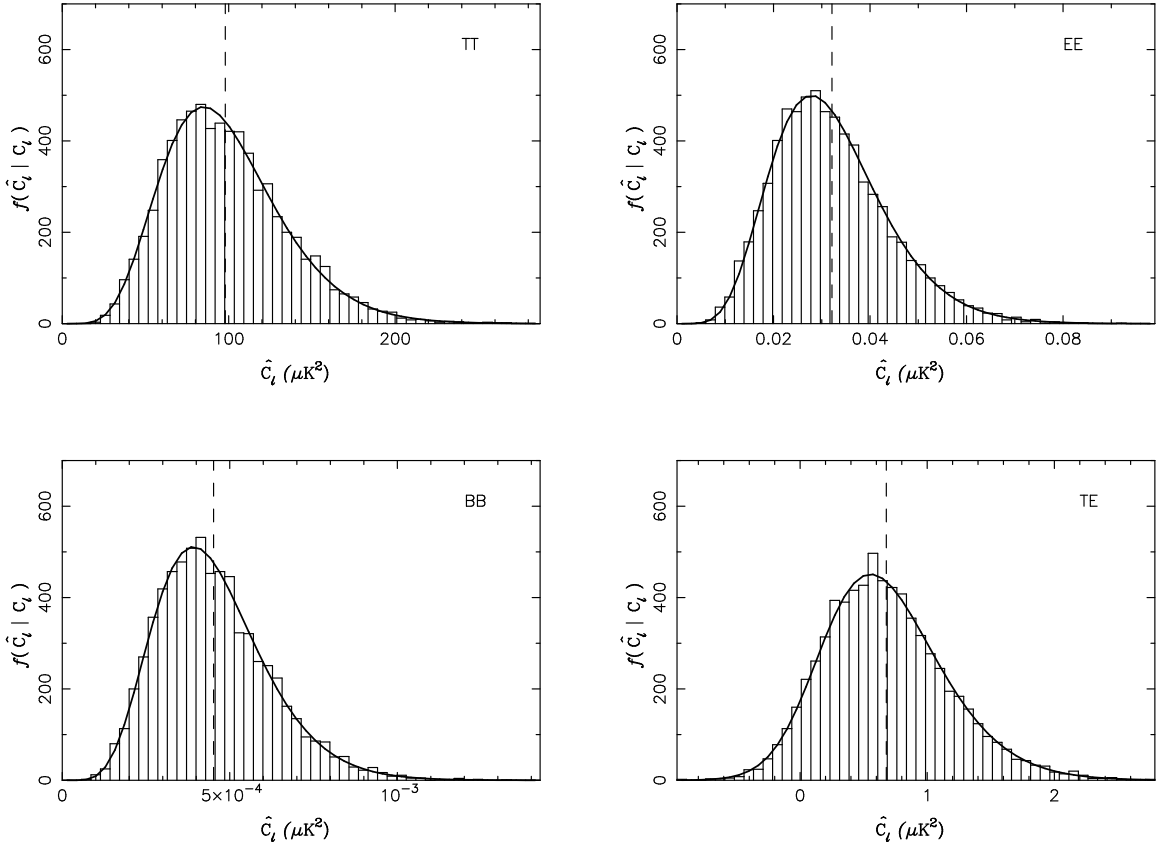


Figure 1. The distribution of recovered $\hat{C}_{l=7}$ calculated for the best-fit cosmological model to the 1-year WMAP data (histograms). A B-mode polarisation component was included in the simulations using a tensor-to-scalar ratio of $T/S = 0.05$. The recovered means, which coincide with the input model spectra, are shown as the vertical dashed lines. These distributions are shown to be in excellent agreement with the predictions provided in Section 3.2 (smooth curves). Note that the marginalised distribution for the TE cross power spectrum more closely resembles a Gaussian distribution than do the Γ distributions of the auto power spectra.

4.1 Partial sky coverage

First we simplify the analysis by ignoring noise and just considering the effect of partial sky coverage. Here, the spherical harmonic coefficients of the cut sky \bar{a}_{lm} are related to the true spherical harmonic coefficients by

$$\bar{a}_{lm} = \sum_{l'm'} K_{lm'l'm'} a_{l'm'}, \quad (22)$$

where $K_{lm'l'm'}$ is a kernel which describes coupling between modes introduced by the non-uniform sky weighting (Hivon et al. 2002; Kogut et al. 2003). It is informative to consider why the Wishart distribution is not valid for these modes. To see this, we focus on the TT power spectrum. For the cut sky coefficients for a particular mode, the estimator, \hat{C}_l^{TT} , equation (4), now sums over a linear combination of the a_{lm} . We can work around correlations between the \bar{a}_{lm} by defining uncorrelated combinations (which must be independent because they also form a multi-variate Gaussian distribution). However, the distribution will consist of variables with differing variance, and therefore does not lead to a Wishart distribution. Additionally, modes at different l will be correlated, again causing deviations from the analysis that led to a Wishart distribution.

The introduction of any sky-cut to a CMB dataset renders the coupling kernel, K of equation (22), singular, and thus prohibits the use of equations (4) & (22) to estimate the underlying power spectra. Various methods have therefore been developed for estimating CMB power spectra from cut-sky datasets, the most prominent of which are the pseudo- C_l (PCL, Hivon et al. 2002) and quadratic maximum likelihood (QML, Tegmark 1997, Bond, Jaffe & Knox 1998) methods.

There are two regimes that we can easily analyse - given a severe sky cut, both the PCL and QML estimators will modify the likelihood distribution from the full-sky Wishart distribution of Section 3.2. However, at large l , the posterior for each mode will remain close to a Gaussian distribution, and we can treat the polarisation and temperature power spectra as a multi-variate Gaussian distribution. In this regime, the error on the recovered coefficients will increase beyond that expected from cosmic variance. In the limit of large l , the fraction of data pairs that remain after applying the sky-cut is equal to the fraction of sky covered f_{sky} . The covariances of the power spectra will therefore be the standard all-sky covariances divided by f_{sky} .

For a modest sky-cut in the limit of low l , the QML estimator is equivalent to the exact estimator of equation (4) with the full-sky a_{lm} 's approximated by

$$a_{lm} = \sum_{l'm'} \bar{K}_{lm}^{-1} \bar{a}_{l'm'}, \quad (23)$$

where \bar{K} is a non-singular matrix formed by truncating the coupling kernel, K of equation (22) at finite values of l' and m' (Efstathiou 2004a). For these modes, data at different l are independent and the likelihood distribution remains a Wishart distribution as described in Section 3.2. In addition, the (co)variances of the QML estimates remain those of equation (21). Clearly, we are going to be interested in both of these regimes, and in analysing data in between. Note that, in this latter regime, the PCL estimator is known to be sub-optimal and the variances of PCL estimates would be significantly increased by estimator-induced variances.

The estimation of \hat{C}_l is obviously coupled with the posterior surface that should be assumed for any model. For instance a ‘‘bias’’ when a Gaussian posterior is assumed is removed when assuming the correct shape of surface. The issue of whether different analysis methods introduce further Gaussian or non-Gaussian noise is more important for our present work.

4.2 Including noise and beam smearing

Here, we consider an all-sky CMB survey, with additive noise, N_l and symmetric Gaussian beam smoothing, B_l . A single (independent) auto-power spectrum measurement can now be written as $D_l = C_l + N_l/B_l^2$, where we have dropped the explicit dependence on TT , EE or BB – when we do this, the formulae are valid for any of these three auto-power spectra. Note that D_l represents measured spectra which have been corrected for the effect of the beam, B_l but have not been corrected for the noise bias, N_l . In the case of uncorrelated Gaussian distributed pixel noise, $N_l = \text{const}$ and our data vector (of which we are calculating the power) is still expected to have a Gaussian distribution. In this case, the marginalised distribution of \hat{D}_l still has a χ^2 form, and the posterior is altered from equation (9), becoming (Bond, Jaffe & Knox 2000)

$$-2 \ln f(D_l|\hat{D}_l) = (2l+1) \left[\ln(C_l + N_l/B_l^2) + \frac{\hat{D}_l}{C_l + N_l/B_l^2} \right]. \quad (24)$$

The curvature around the posterior maximum is

$$-\frac{d^2 f(D_l|\hat{D}_l)}{dC_l dC_{l'}} \propto (C_l + N_l/B_l^2)^{-2} \delta_{ll'}, \quad (25)$$

and the error on our model power spectrum C_l is proportional to $(C_l + N_l/B_l^2)$.

In the case of a joint analysis of temperature and polarisation data, the matrix \mathbf{S}_l , equation (14), will still obey the Wishart distribution of equation (15), but with a revised \mathbf{W}_l matrix given by $\mathbf{W}'_l = \mathbf{V}'_l/(2l+1)$ where \mathbf{V}'_l is now given by

$$\mathbf{V}'_l = \begin{pmatrix} C_l^{TT} + N_l^T/(B_l^T)^2 & C_l^{TE} & 0 \\ C_l^{TE} & C_l^{EE} + N_l^P/(B_l^P)^2 & 0 \\ 0 & 0 & C_l^{BB} + N_l^P/(B_l^P)^2 \end{pmatrix}. \quad (26)$$

In equation (26), we have now allowed for different beam widths (B_l^T & B_l^P) and noise levels (N_l^T & $N_l^{EE} = N_l^{BB} \equiv N_l^P$) for the temperature and polarisation data. Note that for uncorrelated Gaussian distributed noise, the noise cross power spectrum, $N_l^{TE} = 0$. The inclusion of noise and beam smoothing will modify the covariance matrix of the power spectra measurements, equation (21), which becomes (Eisenstein et al. 1999)

$$\mathbf{Y}' = \frac{1}{\nu} \begin{pmatrix} 2(C_l^{TT} + N_l^T/(B_l^T)^2)^2 & 2C_l^{TE}(C_l^{TT} + N_l^T/(B_l^T)^2) & 2(C_l^{TE})^2 \\ 2C_l^{TE}(C_l^{TT} + N_l^T/(B_l^T)^2) & (C_l^{TE})^2 + (C_l^{TT} + N_l^T/(B_l^T)^2)(C_l^{EE} + N_l^P/(B_l^P)^2) & 2C_l^{TE}(C_l^{EE} + N_l^P/(B_l^P)^2) \\ 2(C_l^{TE})^2 & 2C_l^{TE}(C_l^{EE} + N_l^P/(B_l^P)^2) & 2(C_l^{EE} + N_l^P/(B_l^P)^2)^2 \end{pmatrix}. \quad (27)$$

These expressions, which are for the case of uniform uncorrelated pixel noise, are most relevant for satellite experiments where the pixel noise covariance matrix is near-diagonal. Ground-based experiments, in general, have more complicated noise properties and thus require simulations to accurately quantify the posterior distribution for the system.

5 FITTING TO THE POSTERIOR

The complications discussed in the previous section for realistic data, and the deviations from Gaussian behaviour of the posterior discussed in Section 3, can be modelled using a fit to the posterior surface. Such fitting functions can also allow the posterior surface to be approximated without requiring the inversion of a covariance matrix for every model tested – the effect of a varying covariance matrix can be absorbed into the shape of the function. In Section 5.1 we consider a number of possible forms for the posterior fit to a single auto-power spectrum. The extension to include polarisation data is considered in Section 5.2. A good choice of fitting function should be able to interpolate between the posterior distribution in the limit of an all-sky survey at low- l and in the limit of a multi-variate Gaussian distribution at high- l . In order to compare the suitability of different fitting functions, we therefore choose to consider their ability to match the true distributions in these situations. As the inclusion of uncorrelated Gaussian distributed pixel noise does not change the shape of the posterior distributions in either limit, we can ignore its contribution without loss of generality – the effect of noise can be trivially included in both the fits and in the limiting situations that we are testing against.

5.1 Single mode auto-power spectra

We now consider a number of possible fitting functions for the posterior distribution for a single mode of an auto-power spectrum. As in the previous section we will drop the explicit reference to a particular auto-power spectrum, as the formulae and concepts are valid for TT, EE or BB power spectra. We quantify the shapes of different fits using an expansion of the posterior around the maximum $C_l = (1 + \epsilon)\hat{C}_l$ (a variation of the method used in Verde et al. 2003).

For an all-sky, no-noise survey, equation (9) can be expanded to give

$$-2 \ln f(C_l|\hat{C}_l) = \nu \left[\frac{\epsilon^2}{2} - \frac{2\epsilon^3}{3} + O(\epsilon^4) \right], \quad (28)$$

ignoring an irrelevant additive constant. Note that this is not equal to equation 9 in Verde et al. (2003) because of the different expansion adopted (we expand around \hat{C}_l rather than C_l). At first glance, it appears that changing the value of $\nu \equiv (2l + 1)$ does not change the shape of the surface around the maximum as it affects all order terms equally. However, as ν increases, the posterior at a fixed value of ϵ increases. We therefore see that, although the overall shape does not change, the range of parameters with $-2 \ln f(C_l|\hat{C}_l)$ below a fixed value reduces in size and the first order term in ϵ dominates the behaviour. It is in this way that the distribution tends to a Gaussian as $\nu \rightarrow \infty$.

For an all-sky survey, the curvature around the posterior maximum is $2(\hat{C}_l)^2/\nu$. Given a distribution $f(C_l|\hat{C}_l)$, then the first order term in the expansion in ϵ where $C_l = (1 + \epsilon)\hat{C}_l$ should equal $\nu\epsilon^2/2$ in order to match this curvature. The distributions that we now consider as approximations to the posterior surface have all been normalised to match this behaviour to first order. Note that these distributions depend on the model power and therefore intrinsically allow for the model dependence of the variances of the measured power spectra. In this case, a fixed covariance matrix should be used with these posterior fits. An alternative approach would be to recalculate the variance for each model and use an altered posterior shape (Efstathiou 2004b; Challinor & Chon 2005; Brown et al. 2005).

(1) First, we consider a Γ distribution for C_l with degrees-of-freedom equal to μ , thereby matching the shape of the likelihood. We have to be slightly careful as the distribution is usually defined in terms of the mean rather than the maximum. In terms of the maximum, \hat{C}_l , assuming a Γ distribution gives

$$f(C_l|\hat{C}_l) \propto (C_l)^{\mu/2-1} \exp \left[-\frac{(\mu-2)C_l}{2\hat{C}_l} \right], \quad (29)$$

where we have an extra $(\mu-2)/\mu$ term in the exponent compared with equation (6).

This leads to an expansion in ϵ

$$-2 \ln f(C_l|\hat{C}_l) \propto \frac{(\mu-2)}{2} \left[-\ln(C_l/\hat{C}_l) + C_l/\hat{C}_l \right] = (\mu-2) \left[\frac{\epsilon^2}{2} - \frac{\epsilon^3}{3} + O(\epsilon^4) \right]. \quad (30)$$

This distribution is included to emphasise the fact that the posterior does not have the same form as the likelihood – this can easily be seen by comparing equations (28) and (30).

(2) Next, we consider a Gaussian distribution in C_l with fixed variance – chosen to match the curvature around the distribution maximum

$$-2 \ln f(C_l|\hat{C}_l) \propto \frac{\nu}{2(\hat{C}_l)^2} \left[(C_l - \hat{C}_l) \right]^2 = \nu \left[\frac{\epsilon^2}{2} \right]. \quad (31)$$

The mean and maximum of this fit coincide at \hat{C}_l . Most of the distributions that we now consider result from replacing C_l and \hat{C}_l in the right hand side of this expression with functions $g(C_l)$ and $g(\hat{C}_l)$.

(3) For example, setting $g(C_l) = (\hat{C}_l)^2/C_l$ gives

$$-2 \ln f(C_l|\hat{C}_l) \propto \frac{\nu}{2(\hat{C}_l)^2} \left[\frac{\hat{C}_l}{C_l} (C_l - \hat{C}_l) \right]^2 = \nu \left[\frac{\epsilon^2}{2} - \epsilon^3 + O(\epsilon^4) \right]. \quad (32)$$

This distribution could also have been derived from equation (31), by including a factor $(C_l/\hat{C}_l)^2$ to make the variance a function of the model. Note that this distribution is not a Gaussian distribution in C_l with covariances proportional to $(C_l)^2$ – this would require an extra term in the posterior from the effect on the determinant of the covariance matrix. Additionally, this distribution is not the same as a Gaussian in $(\hat{C}_l)^2/C_l$, which would require the inclusion of a Jacobian from the change of variables.

(4) The standard log-normal distribution can be derived by setting $g(C_l) = \hat{C}_l \ln C_l$, to give

$$-2 \ln f(C_l|\hat{C}_l) \propto \frac{\nu}{2(\hat{C}_l)^2} \left[\hat{C}_l \ln(C_l/\hat{C}_l) \right]^2 = \nu \left[\frac{\epsilon^2}{2} - \frac{\epsilon^3}{2} + O(\epsilon^4) \right]. \quad (33)$$

(5) In analogy with equations (31) & (32), we can consider $g(C_l) = (\hat{C}_l)^2 \ln(C_l)/C_l$ (non-standard log-normal).

$$-2 \ln f(C_l|\hat{C}_l) \propto \frac{\nu}{2(\hat{C}_l)^2} \left[\frac{(\hat{C}_l)^2}{C_l} \ln(C_l/\hat{C}_l) \right]^2 = \nu \left[\frac{\epsilon^2}{2} - \frac{3\epsilon^3}{2} + O(\epsilon^4) \right]. \quad (34)$$

This is the distribution obtained by setting the variance to be a function of the model to be tested in the standard log-normal distribution, equation (33).

(6) It is also possible to consider the offset log-normal distribution, where $g(C_l) = \hat{C}_l(1 + a) \ln(C_l + a\hat{C}_l)$

$$-2 \ln f(C_l | \hat{C}_l) \propto \frac{\nu}{2(\hat{C}_l)^2} \left[\hat{C}_l(1+a) \ln\left(\frac{C_l + a\hat{C}_l}{\hat{C}_l + a\hat{C}_l}\right) \right]^2 = \nu \left[\frac{\epsilon^2}{2} - \frac{1}{2(1+a)} \epsilon^3 + O(\epsilon^4) \right]. \quad (35)$$

Setting $a = -1/4$ matches the all-sky no noise behaviour to 2nd order. As $a \rightarrow \infty$, this distribution tends towards Gaussian form.

(7) Because all of our definitions of $g(C_l)$ require the same curvature matrix to match the first order behaviour of the true distribution, we could also consider a combination of 2 or more of them. For example, setting $g(C_l) = aC_l + (1-a)\hat{C}_l \ln C_l$ gives

$$-2 \ln f(C_l | \hat{C}_l) \propto \frac{\nu}{2(\hat{C}_l)^2} \left[a(C_l - \hat{C}_l) + (1-a)\hat{C}_l \ln(C_l/\hat{C}_l) \right]^2 = \nu \left[\frac{\epsilon^2}{2} + \frac{a-1}{2} \epsilon^3 + O(\epsilon^4) \right]. \quad (36)$$

As with the offset log-normal distribution, we can set the free parameter $a = -1/3$ to match the behaviour of the true distribution to 2nd order. For $a \rightarrow 1$, the distribution obviously tends towards a Gaussian form. This distribution, which we suggest calling a summed log-normal distribution, was used by Percival (2005) to model the large-scale structure power spectrum from the 2dF galaxy redshift survey.

(8) An alternative procedure, adopted by Verde et al. (2003), is to combine different posteriors after calculation. Verde et al. (2003) considered combining the posterior \mathcal{P}_1 of equation (32) and the posterior \mathcal{P}_2 of equation (33). Matching the all-sky no-noise posterior shape of equation (28) requires

$$-2 \ln f(C_l | \hat{C}_l) \propto \frac{1}{3} \mathcal{P}_1 + \frac{2}{3} \mathcal{P}_2 = \nu \left[\frac{\epsilon^2}{2} - \frac{2\epsilon^3}{3} + O(\epsilon^4) \right]. \quad (37)$$

We have presented a variety of possible fits to the posterior surface in order to highlight that, even for a single auto-power spectrum, the optimal choice is by no means certain, and will depend on the experiment being analysed.

5.2 Single mode combined temperature-polarisation spectra

We now extend our consideration of fitting formulae for the posterior presented in Section 5.1 to include combined temperature and polarisation data. In this section we only consider a single-mode, and our vector of model power spectra is \mathbf{X}_C , with observed value $\hat{\mathbf{X}}_C$, defined in equation (20).

For an all-sky no-noise survey, the marginalised likelihood distribution for the temperature-polarisation cross-power spectrum \hat{C}_l^{TE} was given in equation (19), and has a form that is different from that of the auto-power spectra. It is therefore clear that the posterior predicted for C_l^{TE} will have a different shape from that of equation (7). In fact, the maximum in the posterior of the marginalised distribution no longer occurs at $C_l^{\text{TE}} = \hat{C}_l^{\text{TE}}$, so we cannot expand the marginalised distribution around the maximum. However, the general Wishart distribution presented in Section 3.2 does predict a maximum in the posterior at $\mathbf{X}_C = \hat{\mathbf{X}}_C$, so we can expand around this point. We can write the posterior distribution as

$$f(\mathbf{X}_C | \hat{\mathbf{X}}_C) \propto \frac{1}{[C_l^{\text{TT}} C_l^{\text{EE}} - (C_l^{\text{TE}})^2]^{\nu/2}} \exp \left[-\frac{\nu}{2} \left(\frac{C_l^{\text{TT}} \hat{C}_l^{\text{EE}} + \hat{C}_l^{\text{TT}} C_l^{\text{EE}} - 2\hat{C}_l^{\text{TE}} C_l^{\text{TE}}}{C_l^{\text{TT}} C_l^{\text{EE}} - (C_l^{\text{TE}})^2} \right) \right]. \quad (38)$$

The curvature matrix around the maximum can be calculated from the second derivatives of this distribution giving

$$\mathbf{Y}_l^{-1} = \frac{\nu}{2[\hat{C}_l^{\text{TT}} \hat{C}_l^{\text{EE}} - (\hat{C}_l^{\text{TE}})^2]^2} \begin{pmatrix} (\hat{C}_l^{\text{EE}})^2 & -2\hat{C}_l^{\text{EE}} \hat{C}_l^{\text{TE}} & (\hat{C}_l^{\text{TE}})^2 \\ -2\hat{C}_l^{\text{EE}} \hat{C}_l^{\text{TE}} & 2[\hat{C}_l^{\text{TT}} \hat{C}_l^{\text{EE}} + (\hat{C}_l^{\text{TE}})^2] & -2\hat{C}_l^{\text{TT}} \hat{C}_l^{\text{TE}} \\ (\hat{C}_l^{\text{TE}})^2 & -2\hat{C}_l^{\text{TT}} \hat{C}_l^{\text{TE}} & (\hat{C}_l^{\text{TT}})^2 \end{pmatrix}, \quad (39)$$

which is the inverse of the covariance matrix given in equation (21) at $\mathbf{X}_C = \hat{\mathbf{X}}_C$.

To compare fitting functions with this distribution, we will adopt the philosophy used in Section 5.1 for independent auto-power spectra, and expand around the maximum. The equations are simplified if we define

$$r = \frac{C_l^{\text{TE}}}{\sqrt{\hat{C}_l^{\text{TT}} \hat{C}_l^{\text{EE}}}}, \quad \hat{r} = \frac{\hat{C}_l^{\text{TE}}}{\sqrt{\hat{C}_l^{\text{TT}} \hat{C}_l^{\text{EE}}}}. \quad (40)$$

First we expand the Wishart distribution in the direction of C_l^{TT} by fixing $C_l^{\text{TE}} = \hat{C}_l^{\text{TE}}$ & $C_l^{\text{EE}} = \hat{C}_l^{\text{EE}}$, and expanding in $C_l^{\text{TT}} = (1+\epsilon)\hat{C}_l^{\text{TT}}$. In this direction,

$$-2 \ln f(C_l^{\text{TT}} | \hat{C}_l^{\text{TT}}) \propto \nu \left[\frac{\epsilon^2}{2} + \frac{2}{3(\hat{r}^2 - 1)} \epsilon^3 + O(\epsilon^4) \right]. \quad (41)$$

In the limit as $\hat{r} \rightarrow 0$, this tends towards the distribution given in equation (28) as expected. By symmetry, expanding C_l^{EE} around \hat{C}_l^{EE} would give the same series expansion (the auto power spectra predict the same posterior shape).

Expanding the Wishart distribution in the direction of C_l^{TE} by fixing $C_l^{\text{TT}} = \hat{C}_l^{\text{TT}}$ & $C_l^{\text{EE}} = \hat{C}_l^{\text{EE}}$, and setting $C_l^{\text{TE}} = (1+\epsilon)\hat{C}_l^{\text{TE}}$ gives

$$-2 \ln f(C_l^{\text{TE}} | \hat{C}_l^{\text{TE}}) \propto \nu \left[\frac{\epsilon^2}{2} + \frac{2\hat{r}^2(\hat{r}^2 + 3)}{3(\hat{r}^4 - 1)} \epsilon^3 + O(\epsilon^4) \right]. \quad (42)$$

For $\hat{r}^2 = 0$, the distribution has a perfect Gaussian form.

We now consider fitting this distribution using multi-variate extensions of the functions discussed in Section 5.1 for auto-power spectra. The expansions in the directions of the auto and cross-power spectra have different shapes, so the *shape* of the fitted distribution for C_l^{TE} must differ from that of C_l^{TT} and C_l^{EE} . The offset log-normal distribution has the flexibility to allow for this change in shape, and we will focus on the multi-variate extension of this distribution. Formally, we will consider a distribution in

$$\mathbf{Z}_C = \begin{pmatrix} \hat{C}_l^{\text{TT}}(1 + a^{\text{TT}}) \ln(C_l^{\text{TT}} + a^{\text{TT}}\hat{C}_l^{\text{TT}}) \\ \hat{C}_l^{\text{TE}}(1 + a^{\text{TE}}) \ln(C_l^{\text{TE}} + a^{\text{TE}}\hat{C}_l^{\text{TE}}) \\ \hat{C}_l^{\text{EE}}(1 + a^{\text{EE}}) \ln(C_l^{\text{EE}} + a^{\text{EE}}\hat{C}_l^{\text{EE}}) \end{pmatrix}, \quad (43)$$

given by

$$-2 \ln f(\mathbf{X}_C | \hat{\mathbf{X}}_C) \propto (\mathbf{Z}_C - \hat{\mathbf{Z}}_C)' \mathbf{Y}_l^{-1} (\mathbf{Z}_C - \hat{\mathbf{Z}}_C). \quad (44)$$

The series expansion of this multi-variate distribution along the standard axes was given in equation (35). Matching this expansion to equations (41) & (42), gives

$$a^{\text{TT}} = a^{\text{EE}} = -\frac{1}{4}(1 + 3\hat{r}^2), \quad a^{\text{TE}} = -\frac{1}{2} \left(2 + \frac{3(\hat{r}^4 - 1)}{2\hat{r}^2(\hat{r}^2 + 3)} \right). \quad (45)$$

The distributions calculated adopting these parameters and the curvature matrix of equation (39) are plotted in Fig. 2, for a basic cosmological model with parameters set at the best-fit values of the simplest 6-parameter model that adequately fits the CMB and 2dFGRS data presented in Sanchez et al. (2006). We present distributions at two wavenumbers $l = 7$, and $l = 100$. Fixing the distribution shape in the directions of the power spectra leaves no free parameters in this simple fit as the covariance matrix is fixed to match the curvature around the peak. In addition to matching the distributions along the power spectra elements of \mathbf{X}_C , the distribution should match the posterior distribution in arbitrary directions in parameter space. In Fig. 2 we therefore also plot the distribution along the principal components of the covariance matrix for these two values of l . As can be seen, fitting the distribution along the power spectra does not constrain the distribution in other directions with the same accuracy. This is an inadequacy of our assumption of replacing the power spectra in equation (31) with a more general function, rather than a problem in the accuracy of the function chosen. We can match the function arbitrarily well in the directions of the power spectra, but the discrepancy in other directions remains. For example, in addition to using the offset log-normal distribution, we have also considered simply defining new variables as the sum of powers of $(C_l^{\text{XX}} - \hat{C}_l^{\text{XX}})$, which can be adjusted to match the distribution to arbitrary order around the maximum. However, even in this case, we find similar problems to those encountered using the offset log-normal distribution. Had we fixed these simple fits in the directions of the principal components, then we would have found problems fitting along the directions of the power spectra. One can, of course, envisage constructing more complicated fitting functions which more accurately reproduce correlations between different power spectra. Such functions would, however, lack the simplicity (and therefore some of the appeal) of fits commonly used to model the temperature power spectrum posterior.

6 MARGINALISING OVER NUISANCE PARAMETERS

For real CMB datasets, one often needs to account for an uncertainty in the calibration of the experiment. This uncertainty is usually considered a nuisance parameter and is marginalised over. For simple assumptions about the form of the underlying power spectrum posterior and of the calibration error, we can perform this marginalisation analytically. Here, we consider the effect of the posterior shape on this marginalisation process. For this analysis, we focus on a single auto-power spectrum. As in previous sections, we drop the explicit dependence on TT , EE or BB when the formulae and derivation are valid for any of these three auto-power spectra.

Consider an experiment where the observed data has a multiplicative ‘‘calibration’’ error, b that is known to have a Gaussian distribution ($\langle b \rangle = 0$, $\langle b^2 \rangle = \sigma_b^2$). If we know the calibration error, then the ‘‘true’’ observed power spectrum value can be recovered, $(\hat{C}_l)_{\text{true}} = (1+b)\hat{C}_l$. The posterior distribution of C_l is then given by

$$f(C_l | \hat{C}_l, \sigma_b) = \int db f(C_l, b | \hat{C}_l, \sigma_b) = \int db f(C_l | \hat{C}_l, b, \sigma_b) f(b | \sigma_b). \quad (46)$$

If $f(C_l | \hat{C}_l, b, \sigma_b)$ has a Gaussian form with variance S then,

$$f(C_l | \hat{C}_l, b, \sigma_b) = \frac{1}{\sqrt{2\pi S}} \exp \left[-\frac{1}{2} (C_l - (1+b)\hat{C}_l) S^{-1} (C_l - (1+b)\hat{C}_l) \right]. \quad (47)$$

This marginalisation can be reduced by ‘‘completing the square’’ (Bridle et al. 2002) to give

$$f(C_l | \hat{C}_l, \sigma_b) = (1 + C_l S^{-1} C_l \sigma_b^2)^{-1/2} f(C_l | \hat{C}_l, b', \sigma_b), \quad (48)$$

where

$$b' = \frac{C_l S^{-1} \hat{C}_l - \hat{C}_l S^{-1} \hat{C}_l}{\hat{C}_l S^{-1} \hat{C}_l + \sigma_b^{-2}}, \quad (49)$$

is the value of the calibration that maximises $f(C_l, b | \hat{C}_l, \sigma_b)$. The offset term $(1 + C_l S^{-1} C_l \sigma_b^2)^{-1/2}$ in equation (48) arises because the variance S is independent of the calibration error.

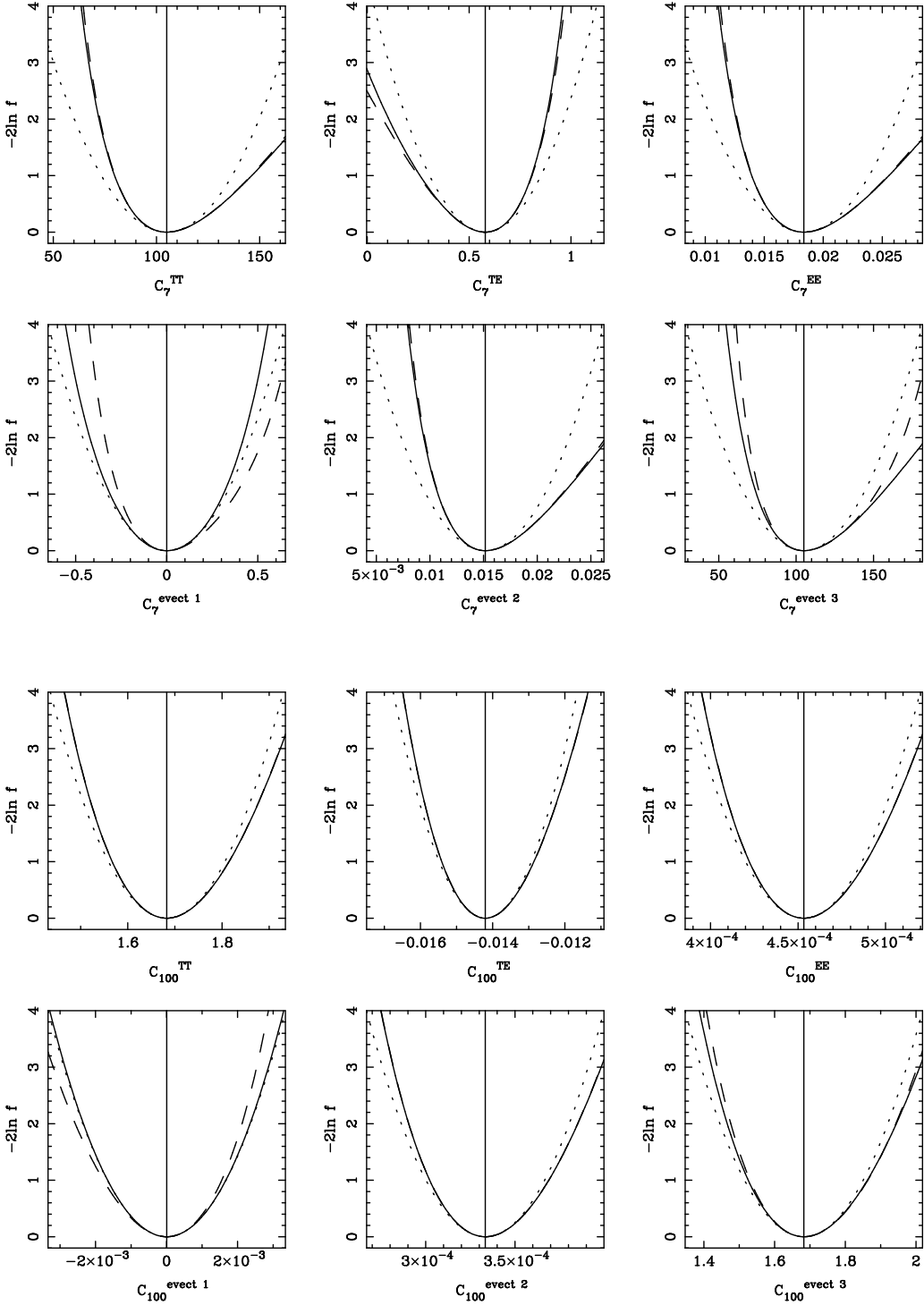


Figure 2. Posterior distributions in different directions in parameter space calculated for the Wishart distribution (solid black line), a simple Gaussian fit to this distribution (dotted line), and a log-normal distribution matched to the Wishart distribution (dashed line). Plots are presented for $l = 7$ (top two rows) and $l = 100$ (bottom two rows). For each value of l , the upper row shows the distribution along the auto and cross-power spectra, while the lower row shows the distribution expanded along the eigenvectors of the covariance matrix. Cosmological parameters were fixed at the best-fit values of the 6-parameter model fitted to the CMB and 2dFGRS data in Sanchez et al. (2006).

The procedure for analytic marginalisation is, however, dependent on the posterior distribution. For an auto-power spectrum of an all-sky no-noise survey, the joint distribution of C_l and b is given by

$$f(C_l, b | \hat{C}_l, \sigma_b) \propto (C_l)^{-\nu/2} \exp \left[-\frac{\nu(1+b)\hat{C}_l}{2C_l} \right] \frac{1}{\sqrt{2\pi}\sigma_b} \exp \left[-\frac{b^2}{2\sigma_b^2} \right]. \quad (50)$$

As in Section 5, we have ignored a contribution from uncorrelated Gaussian pixel noise, which can be easily included as it does not affect the shape of the posterior distribution. Completing the square (as for the Gaussian case above) gives the marginalised posterior,

$$f(C_l|\hat{C}_l, \sigma_b) \propto (C_l)^{-\nu/2} \exp \left[-\frac{\nu(1+2b')\hat{C}_l}{2C_l} \right], \quad (51)$$

where

$$b' = -\frac{\nu\hat{C}_l\sigma_b^2}{2C_l}, \quad (52)$$

is the value of the calibration error that maximises the distribution $f(C_l, b|\hat{C}_l, \sigma_b)$. As can be seen, analytic marginalisation is also trivial when the exact posterior distribution for an all-sky survey is used, rather than a Gaussian. Because of the skewness of this distribution, the result is offset – the value of the calibration error needed to mimic the effect of a full marginalisation is twice that which maximises the likelihood. This demonstrates the difference between marginalisation and simply taking the likelihood maximum.

Our decision to adopt a Gaussian distribution for the calibration error for a single auto-power spectrum measurement was reasonably arbitrary, and we could instead, have considered a calibration error that is Gaussian in the pixel values. When considering the joint likelihood of temperature and polarisation data, the nature of the calibration error becomes increasingly important. For example, assuming independent Gaussian distributed temperature (b^T) and polarisation (b^P) calibration errors would give a calibration error on the TE power spectrum with a distribution based on a modified Bessel function – the distribution of $[(1+b^T)(1+b^P)]^{1/2}$. Obviously, this would complicate the procedure for analytic marginalisation. Additionally, from a single experiment, the temperature and polarisation calibration errors will be highly correlated, which will further increase the complications. Given these issues, there is clearly little to be gained from working through a derivation of analytic marginalisation for combined temperature and polarisation power spectra. For a given experiment, it seems clear that numerical simulations would be required to quantify the effect on the posterior.

7 DISCUSSION

The ultimate goal of CMB experiments is to constrain cosmological models by comparison with theory. In the currently favoured inflationary based cosmological model, the temperature and polarisation fluctuations in the CMB are expected to be isotropic and approximately Gaussian distributed (Liddle & Lyth 2000). In this case, the statistical properties of the CMB can be described completely by the auto- and cross-power spectra of the temperature and polarisation fields. This data compression greatly speeds up the process of comparing with large numbers of theoretical models. In this paper, we have reviewed the mathematical foundation for this comparison. In a Bayesian analysis the posterior, which determines the model constraints, is directly related to the likelihood of a set of data given a particular model; it is therefore important to characterise the likelihood for a given experiment.

For an all-sky survey with uncorrelated Gaussian distributed pixel noise, we have shown that the joint likelihood of the four CMB power spectra is given by a Wishart distribution, a distribution commonly encountered when calculating covariance matrices from Gaussian distributed data. This distribution, which can most easily be written in terms of matrices of the data and model power spectra, provides the likelihood of the measured power spectra including the constraint of positive definiteness. The shape of the likelihood is significantly different from a multi-variate Gaussian at low order multipoles, although it tends towards a multi-variate Gaussian form at high multipoles. The Wishart distribution can be integrated to give marginal distributions for the individual auto- and cross-power spectra. For the auto-power spectra, these marginalised distributions reduce to the well known Γ functions. For the TE cross-power spectrum, the marginalised distribution is more complicated, but can be calculated. We find that the resulting distribution for TE is significantly different to the Γ distributions of the auto power spectra and is closer to (although still differs from) a Gaussian. We have compared the marginalised distributions with those empirically determined from simulated data, finding excellent agreement. Realistically, CMB observations that include polarisation measurements will simultaneously provide constraints on all of the auto- and cross-power spectra. Consequently, the marginal distributions are probably only of academic interest, and we need to consider the combined distribution of all of the different power spectra.

Given the complications of noise and limited sky coverage in real CMB data (discussed in Section 4), the distribution of measured power spectra will, in general, deviate from a Wishart distribution to some degree. However, for a moderate sky cut, it is possible to recover the true temperature auto-power spectrum on large scales. In the case of polarisation data, large uncertainties in the level of polarised foregrounds are currently a limiting factor for CMB experiments. If our understanding of such foregrounds improves sufficiently, then it may be possible to recover the full-sky versions of all four CMB power spectra from future experiments. In that case, the Wishart distribution will be the correct distribution to use for comparing models and data on large scales.

To account for the effect of limited sky coverage on the posterior shape, it has become common practice to model an empirically determined posterior shape using simple fitting functions. We have considered a number of different fits to the posterior for a single auto-power spectrum in Section 5.1, and have extended these simple 1-dimensional fits to cover the combined analysis of temperature and polarisation data. The most commonly used fitting function for auto-power spectra is the offset log-normal distribution. In Section 5.1, it was shown that this is a member of a wider class of models that form a particular extension of the standard Gaussian posterior form. Consequently, the extension of the log-normal distribution to consider the combination of polarisation and temperature data is straightforward, following the natural extension of the Gaussian distribution to a multi-variate Gaussian. A good test of the validity of a fitting function is its ability to match the known posterior distribution for an all-sky survey. For the multi-variate analogue of the log-normal distribution there is a problem, not in its ability to fit to the posterior in the direction of a particular power spectrum, but in fitting correlations between the different power spectra. In fact, we have argued that this problem must be fundamental to the class of models which adopt the same form for the posterior (in the notation of Section 5.2 where some $g(C_l)$ is adopted).

An alternative approach to fitting to the power spectra is to directly fit the pixel data. This has the advantage that the pixel values have

a multi-variate Gaussian distribution and the posterior shape is therefore well known and simple to characterise. However, since it requires the inversion of a $N_{\text{pix}} \times N_{\text{pix}}$ pixel-pixel covariance matrix, this method can only be easily employed on CMB maps with relatively coarse pixelisation, and can therefore only be used to probe the largest scales. To probe smaller scales, more resolution is required and the method rapidly becomes computationally unfeasible with increasing number of pixels. The WMAP team in their 3-year data analysis adopted a hybrid approach where the pixel data were directly fitted on large scales ($l \leq 12$ for temperature and $l \leq 23$ for polarisation), and the TT and TE power spectra were fitted on smaller scales ($l > 12$ and $l > 23$; Hinshaw et al. 2006; Page et al. 2006). On large scales, this has the attractive benefit of avoiding the issues arising from the complicated posterior shape for the power spectra – the real world complications discussed in Section 4 do not distort the likelihood of the pixel values from a multi-variate Gaussian distribution.

In Section 6 we have applied our analysis of posterior shapes to consider marginalisation over nuisance parameters, focusing on an unknown calibration error. Given a form for the posterior distribution, it is possible to perform this marginalisation analytically, leading to a simple correction to the posterior for this “nuisance” parameter. This analytic correction avoids having to explicitly perform the integration. Obviously the analytic form is dependent on the posterior shape, and it has previously been common to assume a Gaussian posterior (Bridle et al. 2002). In Section 6, we provide an additional calculation using the true likelihood of an all-sky survey. Because of the offset nature of this distribution we find a different formula for analytically performing the marginalisation.

The analysis presented in this paper has highlighted the issues involved in a likelihood analysis of combined temperature and polarisation power spectra, and provides the first step on the way to providing a well-characterised method for the fast analysis of combined temperature and polarisation data from future experiments. In subsequent papers we intend to build on this work by considering the practical application of these techniques and the possible modifications needed for analysing upcoming joint temperature and polarisation experiments such as the Planck experiment (Tauber 2004). With the precision with which future experiments will measure the CMB temperature and polarisation fields, the likelihood techniques presented in this paper will become increasingly important for accurately constraining cosmological models from these data.

ACKNOWLEDGEMENTS

WJP and MLB are grateful for support from PPARC fellowships. We acknowledge use of the CMBFAST (Seljak & Zaldarriaga 1996) and HEALPIX (Górski et al. 2005) packages.

REFERENCES

Bennett C.L., et al., 2003, *ApJS*, 148, 1
 Bond J.R., Jaffe A.H., Knox L., 1998, *PRD*, 57, 2117
 Bond J.R., Jaffe A.H., Knox L., 2000, *ApJ*, 533, 19
 Bridle S.L., Crittenden R., Melchiorri A., Hobson M.P., Kneissl R., Lasenby A.N., 2002, *MNRAS*, 335, 1193
 Brown M.L., Castro P.G., Taylor A.N., 2005, *MNRAS*, 360, 1262
 Challinor A., Chon G., 2005, *MNRAS*, 360, 509
 Efstathiou G., 2004a, *MNRAS*, 348, 885
 Efstathiou G., 2004b, *MNRAS*, 349, 603
 Eisenstein D.J., Hu W., Tegmark M., 1999, *ApJ*, 518, 2
 Górski, K.M., Hivon E., Banday A.J., Wandelt B.D., Hansen F.K., Reinecke M., Bartelmann M., 2005, *ApJ*, 622, 759
 Hinshaw G., et al., 2003, *ApJS*, 148, 135
 Hinshaw G., et al., 2006, *ApJS* submitted, astro-ph/0603451
 Hivon E., Gorski K.M., Netterfield C.B., Crill B.P., Prunet S., Hansen F., 2002, *ApJ*, 567, 2
 Kogut A., et al., *ApJS*, 148, 161
 Liddle A.R., Lyth D.H., 2000, “Cosmological Inflation and Large Scale Structure”, Cambridge University Press.
 Page L., 2006, *ApJS* submitted, astro-ph/0603450
 Percival W.J., 2005, *MNRAS*, 356, 1168
 Sanchez A., et al., 2006, *MNRAS*, 366, 189
 Seljak U., Zaldarriaga M., 1996, *ApJ*, 469, 437
 Slosar A., Seljak U., Makarov A., 2004, *PRD*, 69, 123003
 Spergel D.N., et al., 2003, *ApJS*, 148, 175
 Spergel D.N., et al., 2006, *ApJS* submitted, astro-ph/0603449
 Tauber J. A., 2004, *Advances in Space Research*, 34, 491
 Tegmark M., 1997, *PRD*, 55, 5895
 Verde L., et al., 2003, *ApJS*, 148, 195